Applied Catalysis A: General 381 (2010), 242-252

Origin of different deactivation of Pd/SnO_2 and Pd/GeO_2 catalysts in methanol dehydrogenation and reforming: A comparative study

H. Lorenz[1], Q. Zhao[2], S. Turner[3], O. I. Lebedev[3], G. Van Tendeloo[3], B. Klötzer[1], C. Rameshan[1,4], K. Pfaller[5], J. Konzett[6], S. Penner[1,*]

[1]Institute of Physical Chemistry, University of Innsbruck, A-6020 Innsbruck, Austria
[2]School of Materials Science and Engineering, Tianjin University, Tianjin 300072, People's Republic of China
[3]EMAT, University of Antwerp, B-2020 Antwerp, Belgium
[4]Department of Inorganic Chemistry, Fritz-Haber Institute of the Max-Planck Society, D-14195, Berlin, Germany
[5]Section of Histology and Embryology, Medical University Innsbruck, A-6020 Innsbruck
[6]Institute of Mineralogy and Petrography, University of Innsbruck, A-6020 Innsbruck, Austria

[*] Corresponding author: e-mail simon.penner@uibk.ac.at,

Published Online: 15 June 2010

Abstract

Pd particles supported on SnO_2 and GeO_2 have been structurally investigated by X-ray diffraction, (High-Resolution) transmission and scanning electron microscopy after different reductive treatments to monitor the eventual formation of bimetallic phases and catalytically tested in methanol dehydrogenation/reforming. For both oxides this included a thin film sample with well-defined Pd particles and a powder catalyst prepared by incipient wetness impregnation. The hexagonal and the tetragonal polymorph were studied for powder GeO_2. Pd_2Ge formation was observed on all GeO_2-supported catalysts, strongly depending on the specific sample used. Reduction of the thin film at 573 K resulted in full transformation into the bimetallic state. The partial solubility of hexagonal GeO_2 in water and its thermal structural instability yielded Pd_2Ge formation at 473 K, at the cost of a structurally inhomogeneous support and Ge metal formation at higher reduction temperatures. Pd on tetragonal GeO_2 entered a state of strong metal–support interaction after reduction at 573–673 K, resulting in coalescing Pd_2Ge particles on a sintered and re-crystallized support, apparently partially covering the bimetallic particles and decreasing the catalytic activity. Pd_2Ge on amorphous thin film and hexagonal GeO_2 converted methanol primarily via dehydrogenation to CO and H_2.

At 573 K, formation of Pd_2Sn and also PdSn occurred on the Pd/SnO_2 thin film. Pd_3Sn_2 (and to some extent Pd_2Sn) were predominantly obtained on the respective powder catalyst. Strong deactivation with increasing reduction temperature was observed, likely not based on the classical strong metal–support interaction effect, but rather on a combination of missing active structural ensembles on Sn-enriched bimetallic phases and the formation of metallic β-Sn. Correlations to Pd and its bimetallics supported on ZnO, Ga_2O_3 and In_2O_3 were also discussed.

Keywords: Electron Microscopy, Pd_3Sn_2, Pd_2Ge, metal-support interaction, methanol conversion, selected area electron diffraction, Pd_2Sn, PdSn

1. Introduction

Bi-and multi-metallic systems play an ever-increasing role in a variety of research fields ranging from catalysis over electrochemical applications to microelectronics [1]. At least for catalytic studies this also includes Pd-based systems and specifically, also Pd-Sn bimetallics and compounds [2-10]. From the catalytic point of view, Pd-Sn catalysts have been exploited in a number of reactions, including e.g. CO oxidation [2,4,7] or toluene acetoxylation [10] (among others). The specific properties are usually interpreted in terms of a promoting strong metal-support interaction linked to alloy formation between Pd and Sn, leading to an altered noble metal-like electronic structure with respect to clean Pd [9,11]. In contrast, e.g. PdSn alloys on SiO_2 have been shown to be inactive for low-temperature CO oxidation. Catalytic activity was only observed after an additional oxidative annealing step at 673

K and the subsequent formation of Sn-depleted alloys [2]. Naturally, this interest in catalytic activity and selectivity is coupled with the preparation and characterization of different Pd-Sn catalysts. This includes oxide-supported Pd-Sn particles prepared by solvated metal atom dispersion [5], thin film and single-crystal studies [8,9,11] or impregnated systems [2].

Although GeO_2 is increasingly studied for applications in nanostructured devices [12], applications of Ge-containing intermetallic compounds appear to be scarce. Higher selectivities in acetylene hydrogenation over CoGe and Ni_3Ge or in hydrogenation of 1,3-butadiene over Pt_3Ge have been reported [13], but application studies on Pd-Ge systems are virtually non-existent, apart from crystallographic studies concerning formation of specific Pd-Ge bimetallics [14], growth studies of Pd on Ge(001) [15] and investigations on solid-state reactions in Pd-Ge alloy films [16].

Based on studies of Pd-based bimetallic systems supported on the respective oxides and prepared by reduction in hydrogen (i.e. PdZn/ZnO [17], Pd_2Ga and Pd_5Ga_2/Ga_2O_3 [18,19] and $PdIn/In_2O_3$ [20]) as selective catalysts in methanol steam reforming and of the catalytic and structural properties of the respective pure supporting oxides [21-24], the aim of this work was to extend these studies to the corresponding Pd/SnO_2 and Pd/GeO_2 systems. This is partly motivated by the known properties of the Pd-Sn systems but also by the fact that studies on pure SnO_2 and GeO_2 specifically revealed a high CO_2 selectivity of SnO_2 [24,25] and a very low activity and selectivity of GeO_2 in methanol steam reforming [24]. A correlation of catalytic performance of SnO_2 with In_2O_3, and of GeO_2 with Ga_2O_3, has also been established [24], since Sn^{4+} and In^{3+} (and Ge^{4+}, Ga^{3+} and Zn^{2+}) represent isoelectronic species. This analogy of electronic structure may give rise to a potential functional analogy of their catalytic action.

Therefore, it appeared interesting to study if and how the bimetallic formation in both cases considerably improved the CO_2 selectivity. However, due to the reduced activity and/or missing CO_2-selectivity upon entering the bimetallic state, becoming apparent during the studies in methanol steam reforming, the main focus in terms of structure-activity correlations shifted towards a more thorough understanding of the different catalyst deactivation processes.

As already established in our previous work [17-20], a two-way approach will be followed to assess structure-activity/selectivity correlations in the Pd-Sn and Pd-Ge systems. For this reason, thin film model systems prepared on NaCl(001) single crystals will be compared to catalytically more realistic impregnated Pd systems. The former exhibit well-ordered Pd particles with a narrow size distribution and are therefore especially well-suited for structural characterization by electron microscopy [26], but at the same time can also be catalytically examined in a dedicated micro-reactor setup, so that the catalytic properties of thin film and supported catalysts can be directly compared.

2. Experimental

2.1. Catalyst preparation

A high-vacuum chamber (base pressure 10^{-4} Pa) was used to prepare the SnO_2 and GeO_2-supported Pd thin film model catalysts. For preparation of electron microscopy films, Pd metal was deposited by electron-beam evaporation onto a freshly-cleaved NaCl(001) plane at a base pressure of 10^{-4} Pa and a substrate temperature of 623 K (area of the NaCl single crystal about 0.25 cm^2). Subsequently, the Pd particles were either covered by a layer of amorphous or crystalline SnO/SnO_2 or by amorphous GeO_2 (nominal film thickness: 25nm). SnO films were prepared by reactive deposition of SnO_2 powder in 10^{-1} Pa O_2 at 300 K, SnO_2 films by additional post-oxidation at 673 K in 101 kPa O_2. GeO_2 films were prepared by reactive deposition of hexagonal GeO_2 powder in 10^{-2} Pa O_2 at 300 K. As for the catalytic experiments in the micro-reactor larger-area samples are necessary to obtain sufficiently high conversion rates, thin films subsequently used for the catalytic experiments were prepared in the same experiment on freshly deposited NaCl thin films with a larger surface area in a similar way as discussed above. The NaCl thin film supports were prepared by deposition of a polycrystalline NaCl thin film (thickness: 600 nm) at 300 K on two specially designed Cu sheets (37 cm^2 each). The structure of metal particles and support is almost identical on both substrates [27]. For subsequent structural characterization by electron microscopy, the resulting oxide-supported Pd films were floated in distilled water, rinsed and finally mounted on gold grids for electron microscopy. All films used for catalytic measurements were additionally covered by a supporting layer of amorphous SiO_2, prepared by reactive deposition of SiO in 10^{-2} Pa O_2 at 298 K (mean SiO_2 film thickness: 1000 nm). SiO_2 was chosen due to its amorphous nature and its chemical inertness. These films were in turn also floated in distilled water, collected and dried before mounting on quartz wool inside the reactor.

The powder catalyst was prepared by impregnation of the respective oxides with small Pd particles, starting from a water-dissolved Pd precursor salt and commercial or home-prepared oxide powders. These included SnO_2 (Alfa Aesar, 99.99%), hexagonal or tetragonal GeO_2 powder (synthesized from hexagonal GeO_2, Alfa Aesar 99.9999%; see below). After dispersion of the oxides in ~150 ml distilled water, the Pd precursor ($Pd(NO_3)_2$ 99.95%, metals basis, to yield 12 weight-% Pd metal) was slowly added under permanent vigorous stirring. Finally, the water was slowly evaporated and the resulting catalyst subjected to an oxidative treatment in air at 873 K for 1h. This procedure converted the catalysts into PdO/SnO_2 and PdO/GeO_2, as verified by routine X-ray diffraction measurements. A remark on the use of GeO_2 as a catalyst support should be added; as two different crystalline GeO_2 compounds with tetragonal and hexagonal structure exist, which exhibit different solubility in water (the hexagonal is slightly solu-

ble, the tetragonal not [28]), one might experience trouble in preparing the oxide-supported Pd catalysts upon using hexagonal GeO_2 as a catalyst support. This has already been discussed for the pure oxides [24], and structural consequences for the Pd/GeO_2 systems are dealt with in the results section of this paper. Tetragonal GeO_2 was prepared by pressing hexagonal GeO_2 in a gold capsule at 2 kbar and 1000 K for 48 hours using a cold-seal pressure vessel. This procedure transforms the hexagonal phase quantitatively into the tetragonal phase, as verified by XRD [24].

2.2. Catalyst characterization

Reductive and oxidative treatments (101 kPa H_2 or O_2, 1 h) were performed in parallel in a circulating batch reactor in the temperature range between 373-773 K. Structural and morphological changes were followed by (high-resolution) electron microscopy (HRTEM) and selected area electron diffraction (SAED). The electron micrographs were taken with either a ZEISS EM 10C or a JEOL 3000F analytical (scanning) transmission electron microscope (S)TEM operated at 300kV.

The film composition was checked by energy-dispersive X-ray spectroscopy (EDXS). Basically only peaks due to the evaporated elemental thin film constituents (Pd, Sn, Ge and O) and the gold grid (Au) were detected. A small carbon peak, unavoidably with the chosen preparation conditions, is usually present, too. However, we want to point out that this peak remains unchanged during activation or reaction and therefore is not considered a problem. UHV-related surface-sensitive spectroscopic techniques are of limited use since the mounted films are dedicated TEM samples and cannot easily be transferred to a UHV chamber. The purity of the substrate was ensured by freshly cleaving the NaCl(001) crystals immediately before deposition of the oxide. The SAED patterns were calibrated with respect to the Pd (111), (200) and (220) spots in the untreated, as-grown state of the catalysts.

X-ray diffraction experiments were performed ex-situ under ambient conditions using a Siemens D5000 Spectrometer and Cu-K_α radiation (1.54178 Å) at 300 K.

SEM experiments were conducted in an SM 982 GEMINI ZEISS field emission scanning electron microscope. Prior to SEM imaging, the samples were coated with 5 nm Au/Pd to improve its conductance and fixed with conducting carbon paste.

2.3. Catalytic characterization

Catalytic measurements in methanol steam reforming as well as catalyst activation treatments of thin film and powder samples were performed in an NI Labview-automatized re-circulating batch reactor of about 8 ml volume [29].

The catalytic measurements were analyzed using a quadrupole mass spectrometer (Balzers QMG 311) attached to the circulating batch Duran glass reactor via a capillary leak. All methanol steam reforming reactions were conducted with methanol/water mixtures of a 1:9 composition of the liquid phase at room temperature. The gas phase compositions of a variety of different liquid mixtures have been empirically determined by mass spectrometry. On the basis of these measurements we could derive that the volumetric 1:9 mixture corresponds to a gas phase composition of 1:2 = methanol:water at room temperature. All methanol/water mixtures were degassed by repeated freeze-and-thaw cycles. For each catalytic methanol steam reforming experiment, to about 500 Pa methanol/water mixture, 750 Pa Ar (to be measured at m/z = 40) was added to account for the decrease of the mass spectrometer signal due to the continuous gas withdrawal through the leak. Finally, He was added to 101 kPa total pressure.

The molecular masses m/z =2 (H_2), 28 (CO/N_2), 29 ($CH_3OH/HCOOH$), 30 (CH_2O), 31 (CH_3OH/CH_2O), 32 (CH_3OH/O_2), 40 (Ar) and 44 (CO_2), 45 (HCOOH) and 46 (HCOOH) were routinely collected. All mass spectrometer signals of CH_3OH, CO_2, CO, and H_2 were externally calibrated and corrected for fragmentation in the mass spectrometer. This includes m/z = 28 for both CO_2 and CH_3OH and m/z = 45 for CO_2. In order to account for the partial adsorption of methanol and water on the stainless steel parts of the reaction system, all catalytic measurements include a 15 minute equilibration period in the starting mixture prior to each measurement. In each case, the catalyst was exposed to the reaction mixture and the temperature was ramped with 5 K/min to the final value. All the catalytic experiments were additionally corrected for the activity of the catalyst holder containing only quartz wool (almost negligible, at maximum 1 % conversion based on CO_2 formation after 1 h). For data evaluation, the relative intensities of the mass spectrometer signals were converted into partial pressures via external calibration using gas mixtures of defined partial pressures. For simplicity, all catalytic results are usually plotted as partial pressure change versus temperature [20].

3. Results and discussion

3.1. Structural characterization

3.1.1. Thin Films

3.1.1.1. The as-grown states

Figure 1 highlights the as-grown states of the Pd/SnO_x and Pd/GeO_2 catalysts (a,b) along with their SAED patterns (c,d). The Pd particles in both cases are visible as rounded grey and black dots (mean diameter ~9.1 nm and ~8.3 nm, respectively). The light background between the Pd particles is amorphous GeO_2 or SnO_x. The

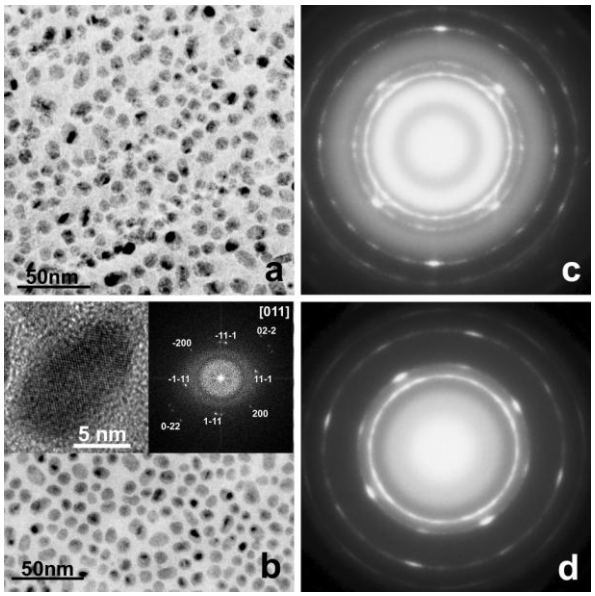

Fig. 1: Overview TEM images of the Pd/SnO_2 (a) and Pd/GeO_2 (b) thin film catalysts. The corresponding SAED patterns are shown in (c) and (d). The inset in Figure c shows a single [011] oriented Pd particle in high resolution.

corresponding SAED patterns (Figure 1 c and d) show the (111), (200) and (220) reflections of the fcc structure of Pd metal, confirming the preferential orientation of the Pd particles along the [001] and [011] zone axes and the well-ordered growth of the Pd particles on NaCl(001). Since both oxides are amorphous, they do not give rise to sharp reflections in the SAED patterns. A HRTEM image of a single as-grown Pd particle on GeO_2 in [011] orientation is shown as a representative example in the inset of Figure 1b.

3.1.1.2. Behaviour upon reduction

For Pd/SnO_x after reduction at 473 K, the mean particle size has increased to about 13.2 nm, but the oxide matrix remains amorphous, as highlighted in Figure 2a. In the SAED patterns however, apart from the diffraction spots of the fcc Pd structure, a new reflection arises at ~ 2.10Å (marked by an arrow), which cannot be addressed to metallic Pd, an eventually crystallized oxide phase (i.e. SnO [30]) or metallic β-Sn [31] (Figure 2c). Enhanced material transport points towards the formation of a Pd-Sn bimetallic phase. This bimetallic formation appears to be complete after reduction at 573 K (Figure 2b and d), where no diffraction spots of metallic Pd persist, but the pattern is better described as an array of diffraction rings with some superimposed elongated spots, pointing to an at least partially well-ordered growth of the bimetallic phase(s), most likely mediated by the structure of the Pd metal. Analysis of the pattern points toward the formation of at least Pd_2Sn

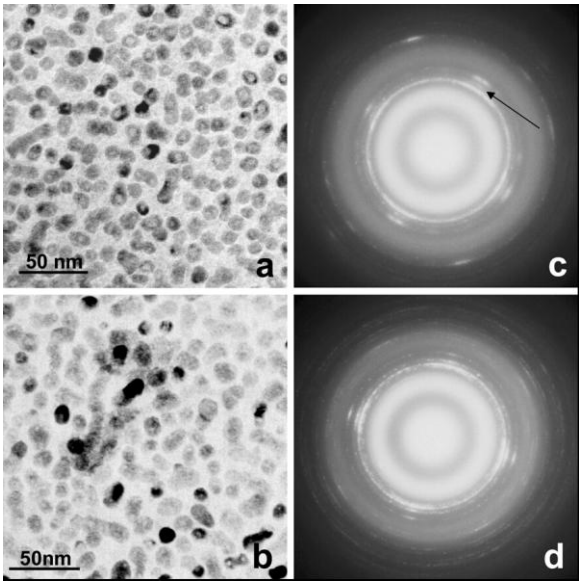

Fig. 2: Overview TEM images of the Pd/SnO_2 after reduction at 473 K (a) and 573 K (b). The corresponding SAED patterns are shown in (c) and (d).

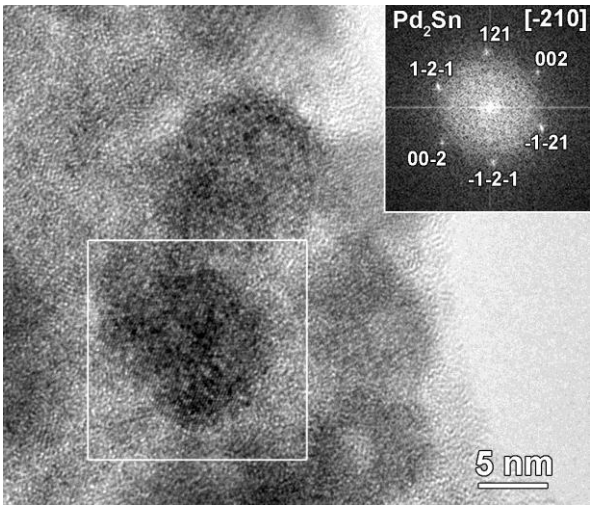

Fig. 3: High-resolution image of a single Pd_2Sn bimetallic particle in [-210] zone axis orientation, formed after reduction at 573 K.

and a second bimetallic phase, most likely PdSn. A complete listing of the observed experimental inter-planar dis tances as well as a possible indexation is given in Table 1. Unfortunately, the phase diagram of Pd-Sn is highly complex in the Pd-rich compositional range between 30 and 40% Sn, which could in principle give rise to the presence of other phases in the same compositional range, e.g. high- and low-temperature modifications of hexagonal Pd_3Sn_2 [32]. The SAED patterns at 573 K can nevertheless consistently be interpreted as a superposition of Pd_2Sn [33] and PdSn [34]. PdSn is identified by its partially ordered reflections arising at d~2.20, 1.92 and 1.54Å, corresponding to the (022), (200) and (040) reflections of the orthorhombic PdSn structure [d_{theor}(022)=2.200 Å, d_{theor}(200)=1.930 Å

Table 1: Interplanar distances d (hkl) [Å] measured on the Pd/SnO_2 and Pd/GeO_2 thin film catalysts in the as grown state and after different reductive treatments. A possible correlation to fcc Pd, hexagonal Pd_2Sn, orthorhombic PdSn and hexagonal Pd_2Ge is also shown.

Pd/SnO_2 as grown		**Pd/SnO_2 red 473 K**		**Pd/SnO_2 red 573 K**		**Pd/GeO_2 as grown**		**Pd/GeO_2 red 573 K**	
d_{exp} [Å]	**d_{theor}[Å]**	**d_{exp} [Å]**	**d_{theor}[Å]**	**d_{exp} [Å]**	**d_{theor}[Å]**	**d_{exp} [Å]**	**d_{theor}[Å]**	**d_{exp} [Å]**	**d_{theor}[Å]**
2.25	2.245 Pd(111)	2.25	2.245 Pd(111)	2.37	2.3600 Pd_2Sn (021)	2.24	2.245 Pd(111)	5.78	5.8100 Pd_2Ge(100)
1.94	1.945 Pd(200)	2.10	2.1100 Pd_2Sn (311)	2.27	2.2800 Pd_2Sn (301)	1.94	1.945 Pd(200)	3.37	3.3560 Pd_2Ge(110)
1.37	1.734 Pd(220)	1.95	1.945 Pd(200)	2.20	2.2010 PdSn (022)	1.38	1.374 Pd(220)	2.91	2.9060 Pd_2Ge(200)
		1.37	1.734 Pd(220)	2.09	2.1100 Pd_2Sn (311)			2.39	2.392 Pd_2Ge(111)
				1.92	1.930 PdSn (200)			2.20	2.1970 Pd_2Ge(210)
				1.73	1.7440 Pd_2Sn (411)			1.94	1.9370 Pd_2Ge(300)
				1.64	1.6460 Pd_2Sn (420)			1.85	1.8460 Pd_2Ge(211)
				1.58	1.5790 Pd_2Sn (231)			1.670	1.7037 Pd_2Ge(002)
				1.54	1.5300 PdSn (040)			1.62	1.6123 Pd_2Ge(310)
				1.40	1.3970 Pd_2Sn (140)			1.51	1.5052 Pd_2Ge(221)
								1.46	1.4573 Pd_2Ge(311)
								1.35	1.3463 Pd_2Ge(212)
								1.28	1.2797 Pd_2Ge(302)
								1.25	1.2418 Pd_2Ge(321)

and d_{theor}(040)=1.530 Å] [34]. These observations are corroborated by the high-resolution TEM image of a single Pd_2Sn particle along the [-210] zone axis (Figure 3). Reduction at temperatures above 573 K leads to strongly enhanced material transport and consequently, a loss of film stability. This observation is also consistent with the formation of Pd-enriched phases at lower reduction temperatures and a transformation to more Sn-enriched phases at higher reduction temperatures.

Reduction of the Pd/GeO_2 thin film model catalyst at 473 K causes a loss of azimuthal ordering, but still only reflections due to the Pd metal phase are present (not shown here). GeO_2 remains amorphous. A different scenario took place after reduction at and above 573 K. As clearly visible in the overview TEM images (Figure 4 a), the mean particle diameter has increased to about 11.3 nm and clear signs of coalescence can be detected, pointing to increased mobility of Pd at these temperatures. The corresponding SAED pattern (Figure 4 c) is a clearly Debye-Scherrer-type ring pattern, exclusively arising from the presence of the hexagonal Pd_2Ge bimetallic phase [35]. No reflections arising from metallic Pd, Ge or crystallized GeO_2 compounds are detectable. After reduction at 673 K, the diameter of the bimetallic particles has increased to ~16.9 nm, but Pd_2Ge is still the only detectable phase (Figure 4b and d). Higher reduction temperatures lead to reductive film destruction. Table 1 again shows a detailed correlation of the measured inter-planar distance with those of the fcc Pd metal structure and the hexagonal Pd_2Ge phase. According to the Pd-Ge phase diagram, Pd_2Ge is the most thermodynamically stable Pd-Ge bimetallic compound [14]. It is worth noting that no *epitaxial* formation of any Pd-Ge bimetallic phase has been observed, which is in striking contrast to Pd particles embedded in ZnO, Ga_2O_3 or In_2O_3 [17-20]. Rather, it resembles Pd particles embedded in amorphous SiO_2 [36]. This behaviour can be rationalized on the basis of the close analogy of the phase diagrams of Pd-Ge and Pd-Si. According to Khalaff et al. [14], both systems exhibit a characteristic low-melting eutectic at Pd-rich compositions and both Pd_2Ge and Pd_2Si are isostructural compounds (hexagonal Fe_2P-type). The similarity between Pd-Ge and Pd-Si is even further pronounced at more Pd-depleted stoichiometries and manifests itself in another very low-melting eutectic around 53 wt% Pd and the subsequent formation of the isostructural MnP-type compounds, namely PdGe and PdSi [14]. In addition, the missing match of the crystal structures of Pd_2Ge or any other Pd-rich Pd-Ge bimetallic and the fcc Pd lattice steers the bimetallic formation towards the thermodynamically most stable Pd_2Ge phase, accompanied by the observed loss of epitaxial orientation.

As outlined in a number of recent publications, this structural coincidence led to the formation of epitaxial PdZn, Pd_5Ga_2 and PdIn bimetallic compounds [17-20],

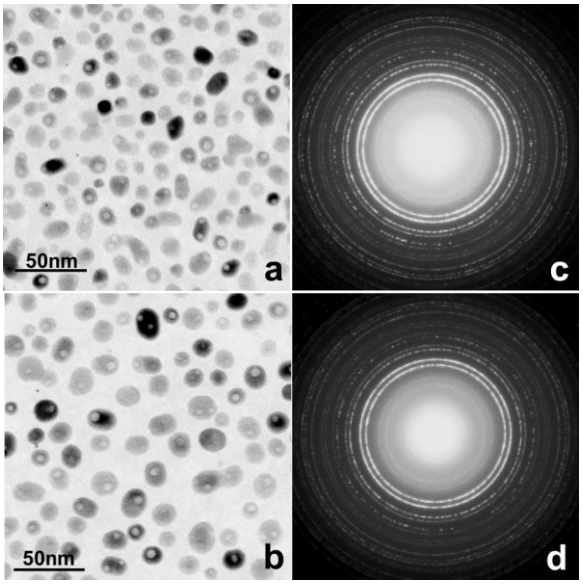

Fig. 4: Overview TEM images of the Pd/GeO_2 after reduction at 573 K (a) and 673 K (b). The corresponding SAED patterns are shown in (c) and (d).

because epitaxy is strongly favoured in these cases. Concerning sintering, Pd/GeO_2 is similar to Pd/Ga_2O_3 and even more to Pd/SiO_2. In all cases, on the thin film models the formation of Pd_2Ge, Pd_2Si [36] and Pd_5Ga_2 [18] bimetallic phases at around 573-673 K is accompanied by considerable particle sintering.

However, one major difference between Pd-Si and Pd-Ge refers to the suppression of hydride formation on Pd-GeO_2 as compared to Pd-SiO_2 [36] and is verified by SAED measurements at reduction temperatures around 523 - 573 K (see Figure 4 a and c). This scenario can be rationalized on the basis of concurring reactions at these temperatures, i.e. (i) reduction of the oxide to form the bimetallic and (ii) Pd β-hydride formation. Obviously, since GeO_2 is thermodynamically less stable than SiO_2 [37], reduction is easier, which in turn favours bimetallic formation at low temperatures over hydride formation, contrary to Pd-SiO_2. [36].

3.1.2. Powder catalysts

3.1.2.1. Pd/SnO_2

To clarify the bimetallic formation on the impregnated PdO/SnO_2 catalysts upon reduction, XRD experiments have been carried out at different reduction stages in the temperature range 373 to 773 K (Figure 5). After calcination in air at 873 K (bottom spectrum), XRD shows the presence of PdO particles, along with strong reflections of the tetragonal cassiterite SnO_2 structure [38]. However, there is a partial overlap between the peaks of the tetragonal PdO and the SnO_2 structure. This especially concerns the strongest PdO(101) reflection at 2.644Å (2Θ=33.875°) [39], which overlaps with the SnO_2(101) peak at 2.649 Å

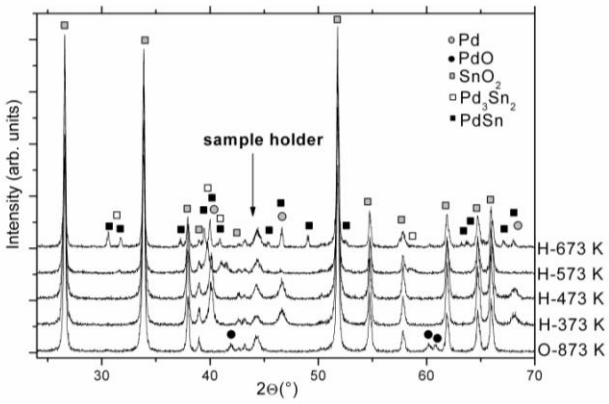

Fig. 5: Set of XRD spectra of the Pd-SnO_2 powder catalyst after different stages of oxidation and reduction.

(2Θ=33.808°) [38]. Reduction of PdO to Pd occurs between 373 and 473 K. At higher temperatures XRD experiments indicate bimetallic formation. Predominant formation of the Pd-rich hexagonal Pd_3Sn_2 phase was observed after reduction at 573 K (marked by open squares) [34]. A small amount of Pd_2Sn was additionally detected in the XRD patterns (at 41.5°/2.176 Å and 46.6°/1.950 Å, the latter corresponding to the (311) lattice spacing of the orthorhombic Pd_2Sn structure. The reflection at 2.176 Å is unassigned [33]). Furthermore, formation of orthorhombic PdSn was observed at 673 K (marked by black squares) [34]. At higher reduction temperatures, a mixture of PdSn, $PdSn_2$ and β-Sn is observed (not shown).

3.1.2.2. Pd/GeO_2

Figure 6 shows the XRD experiments at different stages of reduction. The top panel highlights the experiments on bimetallic formation using tetragonal GeO_2 as support. After calcination at 873 K in air (bottom spectrum) only peaks due to tetragonal PdO and tetragonal GeO_2 are visible (indicated by grey squares and grey circles). Up to 573 K reduction temperature, only peaks due to the fcc Pd and tetragonal GeO_2 are present. Above 573 K, bimetallic formation sets in and hexagonal Pd_2Ge is predominantly formed at 673 K. A small contribution from Pd metal (probably in the particle cores) remains. Unfortunately, the strongest reflections of Pd_2Ge overlap with the peaks of tetragonal GeO_2, e.g. the Pd_2Ge (111) peak at 2.392Å/37.5° or the Pd_2Ge (201) and (210) peaks at 2.211Å/40.8° and 2.197Å/41.1° [35]. The latter two peaks of Pd_2Ge are only visible as a considerable tailing at the lower 2θ side of the GeO_2 peak at ~ 41°. After reduction at 723 K, bimetallic formation led to the formation of an even Ge-richer PdGe bimetallic. This phase is identified by its very small peaks at 3.046 Å, 2.697 Å and 2.165 Å (marked by black squares), corresponding to the (101), (111) and (211) lattice planes of orthorhombic PdGe [40]. However, Pd_2Ge still persists. Both bimetallics can be oxidatively decomposed

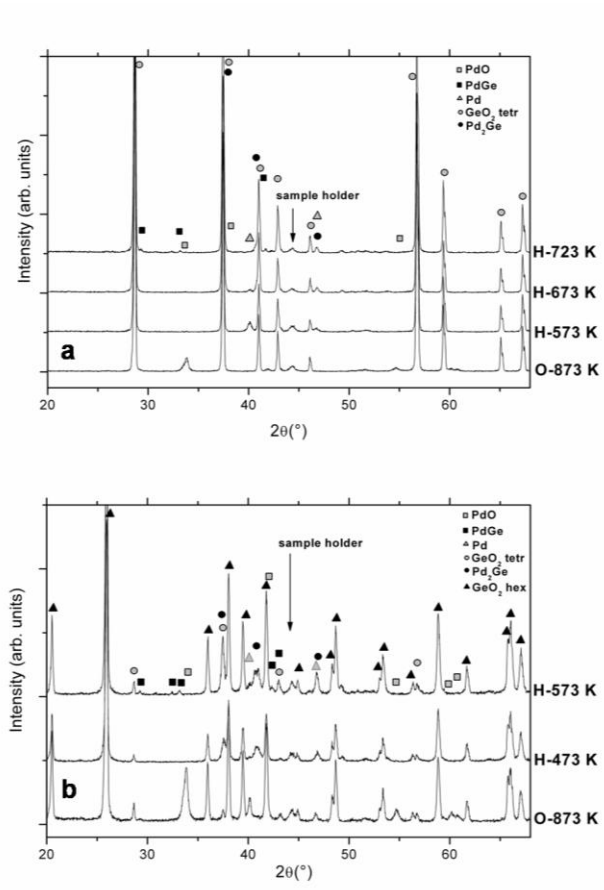

Fig. 6: Set of XRD spectra of the Pd-GeO_2 powder catalyst using tetragonal (panel a) and hexagonal GeO_2 (panel b) as catalyst supports after different stages of oxidation and reduction.

into Pd, PdO and GeO_2 by annealing in 101 kPa oxygen at 723 K for 1h, a prerequisite for catalyst regeneration and catalytic characterization.

The lower panel of Figure 6, highlighting analogous reduction experiments on an impregnated Pd/GeO_2 catalyst, but using hexagonal GeO_2, emphasizes that it is imperative to use tetragonal GeO_2 as catalyst support. Differences to the XRD experiments discussed above are already revealed by the bottom spectrum, corresponding to the unreduced, calcined (i.e. oxidized) catalyst. Strong reflections due to hexagonal GeO_2 [24] and tetragonal PdO [39] are visible. However, due to the slight solubility of hexagonal GeO_2 in water and the subsequent annealing treatment at 873 K, a small portion of the hexagonal GeO_2 phase is transformed into the tetragonal one, as also discussed for pure hexagonal GeO_2 in ref. [24]. As a consequence, even metallic Pd appears in the bottom spectrum, despite the high oxidation temperature of 873 K. This results from dissolution of hexagonal GeO_2 in water and the subsequent encapsulation of a part of the Pd particles by the GeO_2 support after the annealing treatment. Hence, only partial oxidation to PdO occurs. As shown by the other two spectra, taken after reduction at 473 K and 573 K, this is of crucial importance both for bimetallic formation and catalytic characterization. Whereas for Pd/GeO_2 (tetragonal) bimetallic formation set in only after reduction at 673 K (and even in this case some Pd remains), in the case of Pd/GeO_2 (hexagonal) strong reflections of the hexagonal Pd_2Ge phase already appeared after reduction at 473 K and the orthorhombic PdGe phase was already formed after reduction at 573 K. This behaviour is addressed to the larger metal/bimetallic-oxide interface in the case of Pd/GeO_2 (hexagonal) compared to Pd/GeO_2 (tetragonal), induced by the partial encapsulation of the metal particles during catalyst preparation. The onset of bimetallic formation for Pd/GeO_2 (hexagonal) bears some similarities to the bimetallic formation on Pd/GeO_2 thin films, where complete formation of Pd_2Ge has been observed after reduction at 573 K (see above). Since the thin film catalysts also exhibit a much larger metal-support contact area (due to complete embedding of the Pd particles in the oxide matrix) compared to Pd/GeO_2 (tetragonal), the influence and effect of the dimensions of the metal-oxide contact area on bimetallic formation are hence confirmed.

3.2. Catalytic characterization

Figure 7 highlights the methanol steam reforming/dehydrogenation reaction over different Pd/GeO_2 catalysts at various states of reduction. These catalysts included Pd particles embedded in an amorphous GeO_2 matrix (upper panel), supported on hexagonal GeO_2 powder (middle panel) and tetragonal GeO_2 powder (lower panel). The reference state for all catalysts is the state with metallic Pd particles supported on GeO_2, i.e. for the two powder samples after reduction at 373 K, and for the thin film the as-deposited state. As can be seen in the upper panel of Figure 7, denoting the methanol steam reforming/dehydrogenation reaction over a Pd/GeO_2 thin film catalyst after reduction at 373 K (marked by circles), dehydrogenation of methanol started at around 480 K and led to the almost exclusive formation of CO with only little CO_2. This is in agreement with TEM results (see section 3.1.1.2), which indicate metallic Pd at reduction temperatures of 373 K. After reduction at 573 K, however, formation of Pd_2Ge was finished and electron diffraction patterns did not show any metallic Pd remaining. If the Pd_2Ge bimetallic would selectively catalyse the methanol steam reforming reaction, we therefore would expect changes in the selectivity pattern toward CO_2 after reduction at 573 K. Note also that the pure thin film GeO_2 support was observed to be inactive in methanol steam reforming [24]. Catalytic experiments, however, showed exactly the opposite behaviour. Although some sintering occurred already at 573 K, no considerable changes in catalytic activity and selectivity were observed, apart from a delayed onset of methanol dehydrogenation, starting at around 530 K. These results strongly suggest that also over the Pd_2Ge bimetallic, methanol was converted via dehydrogenation and not via steam reforming. Only after reduction at 773 K, deactivation was observed due to reductive film decomposition. In this and the following panels only the CO and CO_2 traces are shown for the sake of

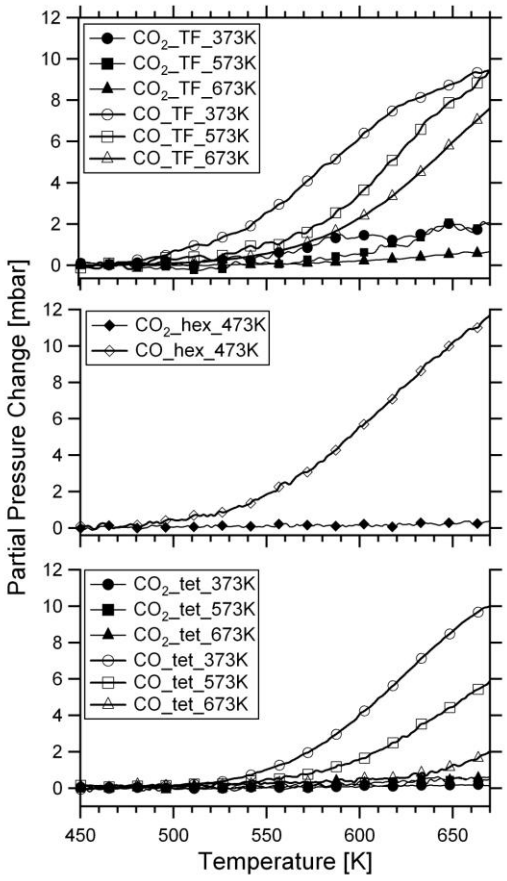

Fig. 7: Methanol dehydrogenation over three different types of Pd-GeO_2 catalysts as a function of reaction temperature. Upper panel: Thin film, middle panel: Pd on hexagonal GeO_2 and lower panel: Pd on tetragonal GeO_2. The temperatures in the legends indicate the pre-reduction temperatures (101 kPa H_2 for 1 h each). Prior to pre-reduction, an oxidative treatment in 101 kPa O_2 at 673 K was applied to all catalysts. Heating ramp: 5 K/min. Sample mass of the powder catalysts: 50 mg

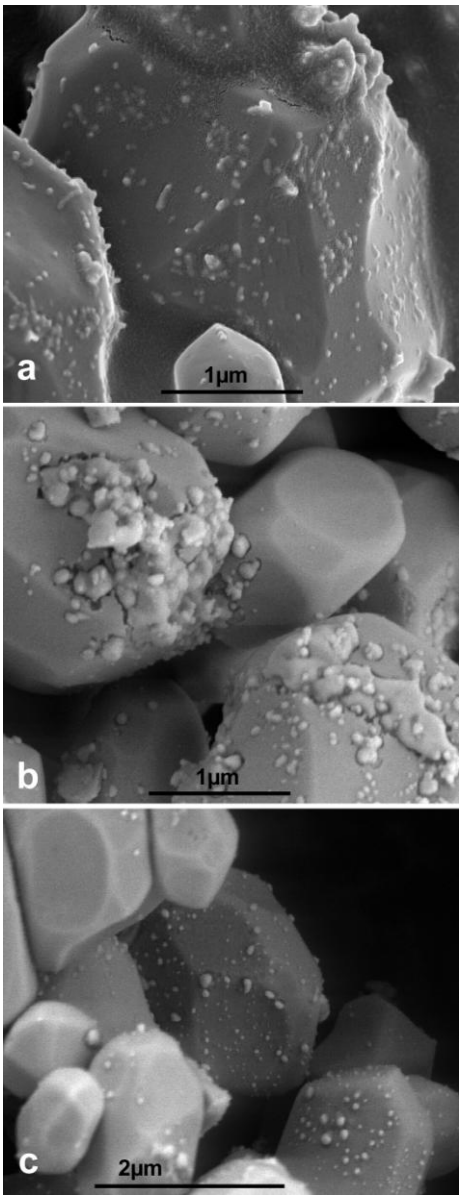

Fig. 8: Scanning electron microscopic images of the powder Pd-GeO_2 (tetragonal) catalyst at different stages of reduction. (a) after calcination at 873 K followed by reduction in 101 kPa H_2 at 373 K for 1 h, (b) after subsequent reduction at 673 K in 101 kPa H_2 for 1 h and (c) after a reduction-oxidation cycle in 101 kPa H_2 at 673 K for 1 h followed by re-oxidation in 101 kPa O_2 at 673 K for 1 h.

clarity. The methanol and hydrogen signals are omitted but they were verified to decrease and increase according to the stoichiometry of the methanol dehydrogenation reaction.

A qualitatively very similar reaction profile was observed on the Pd/GeO_2 (hexagonal) catalyst upon entering the Pd_2Ge bimetallic state after reduction at 473 K (middle panel). Again, only formation of CO was observed at comparable reaction temperatures, with very little CO_2 formed.

On the Pd/GeO_2 (tetragonal) catalyst (bottom panel), however, a different catalytic profile was detected. After reduction at temperatures T ≤ 473 K (metallic Pd is present), methanol dehydrogenation occurred. Raising the reduction temperature to 573 K (still only metallic Pd present according to XRD) yielded a drop in the activity by a factor of two. Reduction at 673 K (where the first peaks of Pd_2Ge appear and almost no metallic Pd remains) deactivated the catalyst almost completely. All changes introduced by reduction were fully reversible upon oxidation at 673 K. Taking together the facts that (i) almost no metallic Pd is present, (ii) XRD indicates the presence of the active Pd_2Ge bimetallic phase, (iii) deactivation is observed and (iv) GeO_2 itself is hardly active, we conclude that some kind of strong metal-support interaction occured between Pd (or Pd_2Ge) and tetragonal GeO_2 after reduction at elevated temperatures. These assumptions are basically corroborated by SEM images of the Pd/GeO_2 (tetragonal) catalyst at different stages of activation. Figure 8 a shows the catalyst after calcination and subsequent reduction at 373 K in 101 kPa H_2 for 1h. Two large GeO_2 grains appear decorated with small Pd particles. Considerable structural alterations are, however, visible after reduction at 673 K (Figure 8 b). Again, some GeO_2 grains are observed, hardly affected by the reduction treatment. Nevertheless, consider

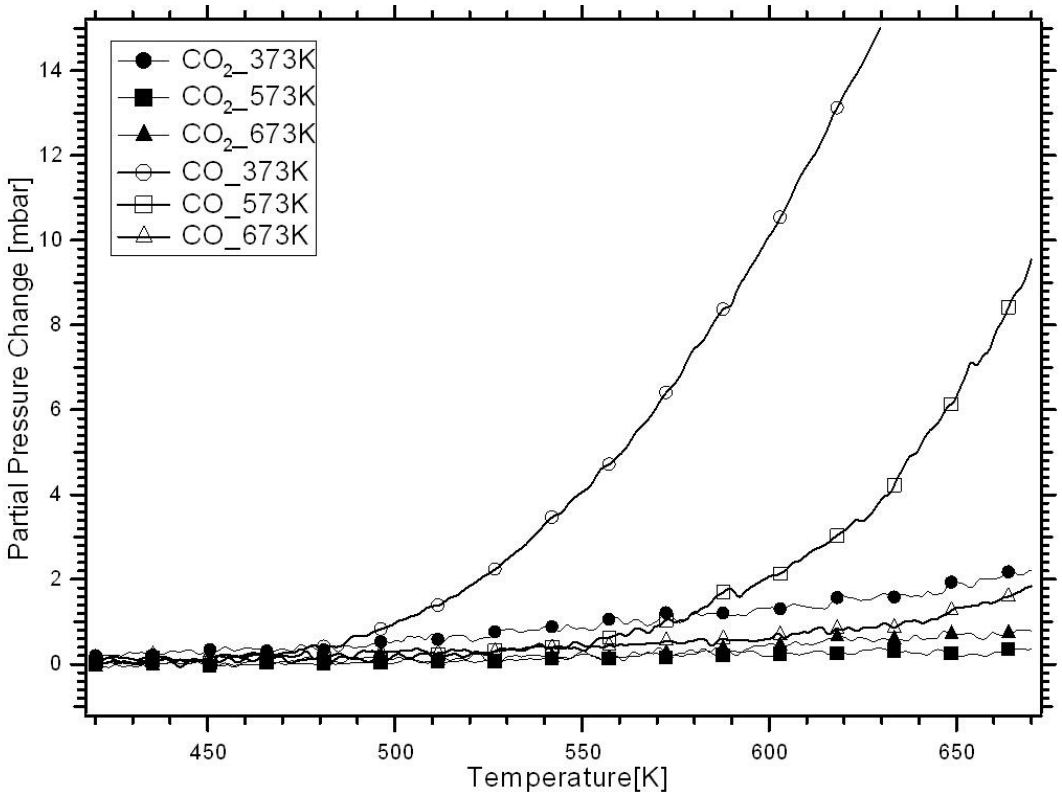

Fig. 9: Methanol dehydrogenation over the Pd-SnO_2 powder catalyst as a function of reaction temperature. The temperatures in the legend indicate the pre-reduction temperatures (101 kPa H_2 for 1 h each). Prior to pre-reduction, an oxidative treatment in 101 kPa O_2 at 673 K was applied to all catalysts. Heating ramp: 5 K/min. Sample mass of the powder catalysts: 50 mg

able agglomeration of the (bi-)metallic Pd particles is easily detectable along with signs of substantial interaction with the GeO_2 support. The Pd-containing particles appear buried and covered by the GeO_2 support, which, at the sites of the former Pd particles, itself appears to be re-crystallized and somehow decorating the sintered (bi-) metallic particles. In any case, this interaction causes the loss of active metal or bimetallic area, leading to the observed drop in the catalytic activity. Figure 8 c, showing the morphology of the catalyst after re-oxidation at 673 K in 101 kPa O_2 for 1 h, indicates re-dispersion of the metallic particles and generally also a re-transformation of the structural alterations of the support towards the state before reduction. As a consequence, also the catalytic dehydrogenation activity was almost fully restored. However, neither on the thin film, nor on the hexagonal GeO_2 such substantial effects were observed, confirming the outstanding behaviour of the tetragonal GeO_2 support.

A different observation in terms of catalyst deactivation upon reduction was made on the SnO_2-supported Pd catalysts. Figure 9 highlights the methanol steam reforming/dehydrogenation experiments as a function of pre-reduction, i.e. bimetallic formation (only the powder experiments are shown, similar observations have been made on the respective thin film model catalysts). Typical methanol dehydrogenation behaviour was observed as long as free Pd metal is available. The traces marked by circles were measured after reduction at 373 K. XRD measurements indicated Pd metal and crystalline SnO_2. From previous studies on the MSR reaction on clean SnO_2 [24], it is known that SnO_2 is active and CO_2-selective (~85%) in its fully oxidized state. However, strong deactivation was observed starting at reduction temperatures of around 523 K, which was explained by the intermediary formation of a SnO surface coating, being subsequently reduced to metallic tin at higher reduction temperatures [24]. In the case of presence of Pd metal, capable of dissociative hydrogen adsorption, higher reduction degrees of the SnO_2 support compared to clean SnO_2 are anticipated at comparable reduction temperatures. Thus, deactivation of the SnO_2 surface by SnO likely occurs at lower temperatures and predominantly methanol dehydrogenation over Pd metal is measured. Strong deactivation of Pd/SnO_2 was also observed after reduction at 573 K (marked by squares), where the predominant formation of Pd_3Sn_2 was deduced from XRD measurements (along with a smaller amount of Pd_2Sn). This deactivation was even more pronounced after reduction at 673 K (marked by triangles). After re-oxidation at 673 K, the activity/selectivity of the initial catalyst was re-established. Two explanations are at hand for this phenomenon: firstly, the observed Pd-Sn bimetallics are inactive for methanol steam reforming/dehydrogenation or secondly, only the “activity” of the support in its highly deactivated state is measured. Substan

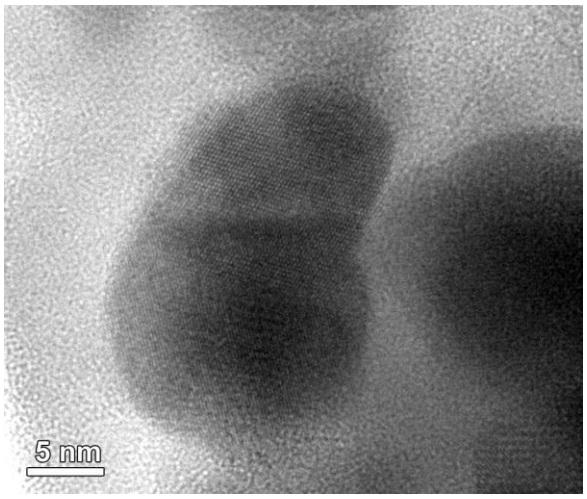

Fig. 10: High-resolution TEM image of Pd-Sn bimetallic powder catalyst particles formed after reduction of the Pd/SnO_2 catalyst at 673 K in 101 kPa H_2 for 1 h, indicating that no decoration of bimetallic particles by SnO_x takes place.

tial contributions from metallic Pd are tentatively excluded since in the XRD spectra only very weak peaks of the Pd fcc structure are observed. For the latter explanation, however, one would have to assume classical strong metal-support interaction of SnO_2 and Pd, where (apart from bimetallic formation) a temporary SnO_x shell encapsulates the (bi-) metallic particles upon reduction, which is again removed upon oxidation. As discussed previously for Pd/In_2O_3 [20], this shell should in principle be visible in high-resolution electron microscopic images. Figure 10 highlights a representative example of two single bimetallic particles (formed after reduction at 673 K) attached to a larger SnO_2 grain. It is immediately clear, that no pronounced shell around the bimetallic particles is present and the lattice fringes of the bimetallic particles extended to the edges [compare with Figure 8 of ref. [20]). Also SEM images of the $Pd\text{-}SnO_2$ catalysts after different stages of reduction are distinctly different from those highlighted in Figure 8 b for $Pd\text{-}GeO_2$ (tetragonal) and show dispersed Pd-Sn particles without considerable agglomeration or interaction with the SnO_2 support. This tentatively leads us to the conclusion that this specific bimetallic situation present after reduction at 573 K (and higher) represents neither an active nor a selective state of the catalyst. It should be emphasized once again that, qualitatively, very similar observations with respect to deactivation have been made on the respective thin film system, where Pd-Sn bimetallics with comparable stoichiometries are formed

The question arises how to explain the deactivation occuring on both Pd-Sn bimetallic catalysts. On the thin film, where the presence of Pd_2Sn (and PdSn) was confirmed by SAED and HRTEM imaging, the deactivation upon the presence of this specific bimetallic can be understood on the basis of CO adsorption measurements on different Pd-Sn surface alloy structures on Pd(111). There, it has been observed, that strong CO chemisorption required the presence of pure Pd three-fold hollow sites, being only present for Pd-enriched multilayer Pd_3Sn surface alloys. Upon formation of an Sn-enriched Pd_2Sn monolayer surface alloy at higher annealing temperatures, the CO chemisorption decreases drastically due to the associated reduction of the number of available active "Pd_3" ensembles [41]. Similarly, the presence of Pd_2Sn has shown to strongly suppress the activity in cinnamaldehyde hydrogenation [6]. In addition, formation of Sn-enriched Pd-Sn phases was also suspected to decrease the activity of $Pd\text{-}SnO_2$ catalysts in crotonaldehyde hydrogenation [5]. Specifically, PdSn particles on SiO_2 were found to be inactive for low-temperature CO oxidation [2]. In a corresponding line of argumentation, the presence of Pd_2Sn and PdSn bimetallic particles on the thin film and predominantly Pd_3Sn_2 on the powder catalyst, or generally, Sn-enriched bimetallic phases, may also effectively suppress the adsorption and dissociation of methanol molecules on specific Pd-Sn ensembles, required for further methanol conversion.

Another point which puts $Pd\text{-}SnO_2$ apart from the other studied systems, is the higher propensity of SnO_2 to be reduced down to the metallic β-Sn state [28]. From all the other oxides studied (ZnO, Ga_2O_3, In_2O_3, GeO_2), SnO_2 is the only one being reduced to Sn metal even in the presence of a water partial pressure in the mbar range. E.g. In_2O_3 requires completely dry, flowing hydrogen for reduction toward the metallic state, because reduced In species are easily re-oxidized by water. Recalling the XRD spectra of $Pd\text{-}SnO_2$ after reduction at 673 K, we note two peaks at 30.5°/2.911 Å and 31.7°/2.816 Å, which are addressed to the (111) and (012) reflections of the orthorhombic PdSn phase [34] and are, among others, used to identify this phase (see section 3.1.2.1). Identifying metallic β-Sn on this specific sample is not straightforward, since the two most prominent peaks of β-Sn at 30.63°/2.915 Å and 32.02°/2.790 Å, corresponding to the (200) and (101) lattice spacing of its tetragonal structure [31], overlap with the two PdSn reflections mentioned previously, and two other more intense peaks of metallic β-Sn (at 43.88°/2.061 Å and 44.91°/2.017 Å, corresponding to the (220) and (211) lattice spacings [31]) overlap with the reflections of the sample holder. The presence of metallic tin is, however, confirmed after reduction at 773 K, since then these metallic peaks are very well pronounced and can more easily be distinguished especially from those of the sample holder. As a consequence, we cannot fully exclude the presence of metallic Sn additionally spoiling the catalytic activity already after reduction at 673 K.

4. Summary and conclusions

We successfully extended the studies conducted previously on $Pd\text{-}Ga_2O_3$ and $Pd\text{-}In_2O_3$ [18-20] to the respective oxides of the 4th main group of the periodic table. Structural similarities include the generally easy preparation of the oxide-supported bimetallic state and for $Pd\text{-}GeO_2$, the formation of a single bimetallic phase at low reduction tem-

peratures. However, the special properties of the oxides upon annealing and reduction are suspected to introduce another level of difficulty in metal/bimetallic-support interaction and consequently also in the interpretation of catalytic activity and selectivity. For the Pd-GeO_2 system we studied these effects for three different GeO_2 supports, namely an amorphous thin film and a crystalline hexagonal and tetragonal phase. Although Pd_2Ge as the thermodynamically most stable Pd-Ge bimetallic compound is formed with all supports, the preparation conditions have been shown to crucially depend on the specific oxide properties. Full transformation to Pd_2Ge has been observed at 573 K on the thin film. Hexagonal GeO_2 is only of limited use as support since its ability to partially dissolve in water and its easy partial transformation into the tetragonal phase leads to the formation of Pd_2Ge at 473 K. Pd on tetragonal GeO_2 appears to be severely affected by strong metal-support interaction effects at higher reduction temperatures. Consequently, the activity of the Pd_2Ge bimetallic in methanol steam reforming could only be studied on the hexagonal and amorphous supports. Methanol dehydrogenation was identified as the dominant reaction pathway.

A different form of deactivation upon entering the bimetallic state has been observed on Pd-SnO_2, because the structural extent of deactivating strong metal-support interaction is less apparent as compared to Pd/GeO_2 (both on the thin film and the powder sample). A decoration layer of reduced SnO_x is not present after reduction. Therefore, the decrease of the number of necessary structural Pd ensembles for methanol adsorption and dissociation upon formation of Sn-enriched bimetallics is considered as a possible form of deactivation, as shown previously e.g. for CO adsorption/oxidation and conversion of α,β-unsaturated aldehydes. Formation of metallic β-Sn must also be considered as a possible source of decreasing the catalytic activity in methanol reactions. Compared to In_2O_3 or Ga_2O_3, however, the discrimination of the activity between bimetallic phase and reduced oxide is not straightforward, since In_2O_3 and Ga_2O_3 are still active after reduction, but SnO_2 under comparable experimental conditions, is not. This hampers the "catalytic" detection of a possible shell of reduced SnO_x after reduction.

Apparently, Pd supported on both SnO_2 and GeO_2 never yields CO_2-selective oxide-supported bimetallic methanol steam reforming catalysts under any experimental conditions, in contrast to Pd-ZnO, Pd-Ga_2O_3 and Pd-In_2O_3

Acknowledgements

The authors are grateful to the FWF (Austrian Science Foundation) for financial support under project P20892-N19. The authors acknowledge support from the European Union under the Framework 6 program under a contract from an Integrated Infrastructure Initiative (Reference 026019 ESTEEM). Q. Zhao thanks the Eurasia-Pacific Uninet for a scholarship award.

References

[1] J. A. Rodriguez, Surf. Sci. Rep. 24 (1996) 223-287
[2] J. Arana, P. Ramirez de la Piscina, J. Llorca, J. Sales, N. Homs, J.L.G. Fierro, Chem. Mater. 10 (1998) 1333-1342
[3] A. Pintar, J. Batista, I. Musevic, Appl. Catal. B 52 (2004) 49-60
[4] A. D. Logan, M. T. Paffett, J. Catal. 133 (1992) 179-190
[5] G. Cardenas, R. Oliva, P. Reyes, B. L. Rivas, J. Mol. Catal.A 191 (2003) 75-86
[6] A. Hammoudeh, S. Mahmoud, J. Mol. Catal. A 203 (2003) 231-239
[7] B. Mirkelamoglu, G. Karakas, Appl. Catal. A 281 (2005) 275-284
[8] S. Nemsak, K. Masek, V. Matolin, Surf. Sci. 601 (2007) 4475-4478
[9] N. Tsud, V. Johanek, I. Stara, K. Veltruska, V. Matolin, Thin Solid Films 391 (2001) 204-208
[10] S. K. Tanielyan, R. L. Augustin, J. Mol. Catal. 90 (1994) 267-289
[11] N. Tsud, T. Skala, F. Sutara, K. Veltruska, V. Dudr, S. Fabik, L. Sedlacek, V. Chab, K. C. Prince, V. Matolin, Surf. Sci. 595 (2005) 138-150
[12] V. V. Atuchin, T. A. Gavrilova, S. A. Gromilov, V. G. Kostrovsky, L. D. Pokrovsky, I. B. Troitskaia, R. S. Vemuri, G. Carbajal-Franco, C. V. Ramana, Cryst. Growth Des. 9 (2009) 1829-1832 and references therein
[13] T. Komatsu, K. Sou, K. Ozawa, J. Mol. Catal. A: Chem. 319 (2010) 71-77
[14] K. Khalaff, K. Schubert, Z. Metallkde 65 (1974) 379-382
[15] J. Wang, M. Li, E. I. Altman, J. Appl. Physics 100(11) (2006) 113501/1-113501/7
[16] Z. Chen, S. Zhang, S. Tan, Z. Wu, Mater. Sci. Eng. A(373(1-2) (2004) 21-25
[17] S. Penner, B. Jenewein, H. Gabasch, B. Klötzer, D. Wang, A. Knop-Gericke, R. Schlögl, K. Hayek, J. Catal. 241 (2006) 14-19
[18] S. Penner, H. Lorenz, B. Klötzer, D. Wang, M. Stöger-Pollach, C. Rameshan, W. Jochum Appl. Catal. A 358 (2009) 193-202
[19] H. Lorenz, S. Penner, B. Klötzer, C. Rameshan, W. Jochum, Appl. Catal. A 358 (2009) 203-210
[20] H. Lorenz, O. Lebedev, S. Turner, B. Klötzer, Ch. Rameshan, K. Pfaller, S. Penner Appl. Catal. A 374 (2010) 180-188
[21] H. Lorenz, M. Stöger-Pollach, S. Schwarz, J. Bernardi, K. Pfaller, B. Klötzer, S. Penner Appl. Catal. A 347 (2008) 34-42
[22] H. Lorenz, M. Stöger-Pollach, S. Schwarz, J. Bernardi, K. Pfaller, B. Klötzer, S. Penner J. Phys. Chem. C 112 (2008) 918-925
[23] S. Penner, B. Klötzer, B. Jenewein, X. Liu, E. Bertel, F. Klauser, Thin Solid Films 516 (2008) 4742-4279
[24] Q. Zhao, H. Lorenz, O. Lebedev, S. Turner, G. van Tendeloo, C. Rameshan, B. Klötzer, J. Konzett, S. Penner, Appl. Catal. A 375 (2010) 188-195
[25] A. Neramittagapong, S. Hoshino, T. Mori, J. Kubo, Y. Morikawa, Chem. Lett. (2002) 1078-1079

[26] G. Rupprechter, K. Hayek, L. Rendon, J.M. Yacaman, Thin Solid Films 260 (1995) 148-155
[27] G. Rupprechter, K. Hayek, H. Hofmeister, J. Catal. 173 (1998) 409-422
[28] R. J. Meyer, Gmelins Handbuch der Anorganischen Chemie, 8. Auflage, 1958, Verlag Chemie, GmbH Weinheim/Bergstrasse
[29] C. Zimmermann, K. Hayek, Chem. Ing. Tech. 63 (1991) 221-230
[30] F. Izumi, J. Solid State Chem. 38 (1981) 381-385
[31] J. A. Lee, G. V. Raynor, Proc. Phys. Soc., London, 67 (1954) 737-747
[32] Landolt-Börnstein, Phase equlibria, crystallographic and thermodynamic data of binary alloys, Group IV/Volume 5, Springer 1998, Berlin
[33] A. D. Genkin, T.L. Evstigneeva, L.N. Vyal'sov, I.P. Laputina, and N.V. Groneva, Geol. Rudn. Mestorozhd., 16 (1974) 98–103
[34] Nowotny, G. Schubert, A. Dettinger, Metallforschung 4-5 (1946) 137-145
[35] W. Wopersnow, G. Schubert, J. Less-Common Met. 52 (1977) 1-12
[36] B. Jenewein, S. Penner, H. Gabasch, B. Klötzer, D. Wang, A. Knop-Gericke, R. Schlögl, K. Hayek, J. Catal. 241 (2006) 155-161
[37] Ihsan Barin, Thermodynamic Data of Pure Substances, VCH, 1993, Weinheim
[38] W. Baur, Acta Crystallogr. A 9 (1956) 515-520
[39] Swanson et. al. Natl. Bur. Stand. (US), Circ. 539 IV, 27 (1955)
[40] H. Pfisterer, K. Schubert, Z. Metallkde 41 (1950) 358-363
[41] A. F. Lee, C. J. Baddeley, M. S. Tikhov, R. M. Lambert, Surf. Sci. 373 (1997) 195-209